The Hamilton-Jacobi method and Hamiltonian maps

2002 J. Phys. A: Math. Gen. 35 2811

(http://iopscience.iop.org/0305-4470/35/12/307)

INSTITUTE OF PHYSICS PUBLISHING JOURNAL OF PHYSICS A: MATHEMATICAL AND GENERAL

J. Phys. A: Math. Gen. **35** (2002) 2811–2832 PII: S0305-4470(02)27768-9

The Hamilton–Jacobi method and Hamiltonian maps

S S Abdullaev

Institut für Plasmaphysik, Forschungszentrum Jülich GmbH, EURATOM Association, Trilateral Euregio Cluster, D-52425 Jülich, Germany

Received 3 August 2001, in final form 15 February 2002
Published 15 March 2002
Online at stacks.iop.org/JPhysA/35/2811

Abstract
A method for constructing time-step-based symplectic maps for a generic Hamiltonian system subjected to perturbation is developed. Using the Hamilton–Jacobi method and Jacobi's theorem in finite periodic time intervals, the general form of the symplectic maps is established. The generating function of the map is found by the perturbation method in the finite time intervals. The accuracy of the maps is studied for fully integrable and partially chaotic Hamiltonian systems and compared to that of the symplectic integration method.

PACS numbers: 05.45.Ac, 05.60.Cd, 52.25.Fi

Mathematics Subject Classification: 37E40, 37J10, 37J40, 37M15, 70H09, 70H20

1. Introduction

Many fundamental problems of physics and mechanics, whenever a dissipation is not significant, may be modelled by Hamiltonian systems [1–3]. An n-degree-of-freedom system can be described by $2n$ ordinary differential equations of first order in the phase space of the canonical coordinates (p, q), canonical momenta $p = (p_1, \ldots, p_n)$, and coordinates $q = (q_1, \ldots, q_n)$. One of the features of the Hamiltonian system is that it conserves certain invariants in phase space, e.g., the symplectic form. In a numerical study of Hamiltonian systems, it is important to preserve this property.

The standard numerical method used to integrate the system of ordinary differential equations is not ideal for this purpose, because the numerical approximations introduce non-Hamiltonian perturbations which lead to completely different long-term behaviour. For this reason, special integration tools, known as symplectic integrators, have been developed for the numerical study of Hamiltonian systems (see, for example, the reviews [4–6]). The methods based on these preserve the properties of Hamiltonian systems by arranging each integration step to be a canonical transformation. Symplectic integration methods play an important role in the study of the long-time evolution of Hamiltonian systems.

Symplectic maps constitute another powerful tool for studying Hamiltonian systems [3, 7–9]. The maps are inherently constructed in the symplectic form, and thus they always preserve the important properties of Hamiltonian systems. This approach is ideal for studying the long-term evolution of a system, and especially in cases where the system exhibits chaotic behaviour where there is an exponential divergence of orbits with close initial coordinates in phase space. The symplectic maps have been successfully employed in many problems of astronomy, plasma physics, fluid dynamics, accelerator physics, etc [3, 9–12].

Magnetic field lines provide an excellent example of a Hamiltonian system [13, 14]. The flux-preserving property of the magnetic field is then formulated as symplecticness of the Hamiltonian system. It allows one to model magnetic field lines in magnetic confinement devices, such as tokamaks and stellarators, by flux-preserving maps [15–29]. The symplectic maps have also been used to study the transport and mixing processes in plasmas [30, 31] and in structured fluids containing a variety of vortices, waves, jets, and fronts [32–37]. They are also extensively employed in the simulation of single-particle motion in accelerators [38, 39]. Symplectic maps for the N-body problem have been proposed for the long-term evolution of planetary systems in dynamical astronomy [40–42].

In spite of the extensive use of symplectic maps in many Hamiltonian problems during last four decades, the derivation of symplectic maps from the Hamiltonian equations remains elusive. There are several approaches for constructing symplectic maps. One approach is based on the *a priori* assumption that the map has a symplectic form, and the generating functions associated with the map are found from the equations of motion [3, 16, 18, 25, 38]. The well-known *perturbed twist maps* have been obtained in such a way.

Another method for constructing symplectic maps is based on the assumption that a time-periodic perturbation acting on the integrable system may be replaced by periodic delta functions, which is equivalent to adding fast-oscillating terms to the perturbed Hamiltonian. This is justified by the averaging principle, i.e., by the fact that if the non-resonant high-frequency terms do not play a noticeable role in the dynamics of the system, then adding these terms does not significantly affect the evolution. The integration of the equations of motion along delta functions gives such symplectic maps, with the time step equal to the period of the perturbation [7, 40–43]. In particular, this method was used by Chirikov to derive the celebrated *standard map* [7].

However, these methods of derivation of maps have significant shortcomings. The former approach restricts possible symplectic forms of the maps and does not allow one to obtain higher-order corrections to the generating function.

The use of delta functions causes, in general, other difficulties in the derivation of maps. In many physical systems one studies a motion subjected to periodic perturbation in time (or in space) with a broad spectrum of modes. Simple replacement of these perturbations by one with an infinite number of modes gives rise periodic delta functions in time (or in space). Such a procedure introduces artificial singularities and discontinuities which were not present in the original system, and leads, in general, to the some uncertainty in the form of the maps because of the poorly defined procedure of integration along the delta functions: a different asymptotic representation of the delta function may give rise to a different form of map. For instance, as was shown in [44], a symmetric representation of the delta function leads to a symmetric form of the symplectic map. It turns out that the latter more closely describes the Hamiltonian system than the asymmetric form of map known as the perturbed twist map.

Moreover, both approaches are unable to obtain the higher-order corrections to maps and therefore to provide an estimate of the accuracy of the maps. The most serious deficiency of the methods is that they cannot clearly distinguish between the map variables and those of the original system. It is simply assumed that these variables are identical.

A rigorous method for constructing Hamiltonian maps which does not have the above-mentioned shortcomings has been recently proposed in [45, 46]. It is based on the method of canonical change of variables which eliminates the perturbation in periodic time intervals. This procedure transforms the perturbed system to a new one for which the motion is unperturbed during the entire period except at discrete periodic time instants where all perturbation act instantaneously as kicks. The relations between variables in the neighbouring time intervals are found by making an inverse canonical change of variables to the old variables. In this way, one can establish a symplectic mapping describing the evolution of the system's old variables in one period of perturbation. The changes of variables are given by generating functions satisfying the Hamilton–Jacobi equations, which are solved using perturbation theory.

In the present work we develop a general method for constructing symplectic maps for a Hamiltonian system with the arbitrary time steps. We will consider a generic Hamiltonian system which may be presented as a sum of a completely integrable system and a Hamiltonian perturbation. The perturbed part of the Hamiltonian is not necessarily small. Using the Hamilton–Jacobi method—in particular Jacobi's theorem—allows one to construct a symplectic map by means of the canonical change of variables in a clear and transparent way. The generating functions associated with the map are found by solving the Cauchy problem for the Hamilton–Jacobi equations using the perturbation theory in finite time intervals. The perturbation series for the generating functions obtained in this way does not contain divergent terms due to *small denominators* (or *small divisors*), unlike the classical perturbation series in an infinite time domain which represents the main difficulty encountered in the classical perturbation theory (see [1, 2, 47, 48]).

One of the advantages of the method is that the accuracy of the mapping method does not depend on the oscillation frequency of the system. This makes the method a very convenient tool for integration of highly oscillatory Hamiltonian systems, unlike the standard symplectic integrators whose accuracy deteriorates with the increase of the oscillation frequencies.

The paper consists of six sections and an appendix. In section 2 the basis of the Hamilton–Jacobi method is recalled and the construction of the Hamiltonian maps using Jacobi's theorem is presented. The perturbation theory used for solving the Hamilton–Jacobi equation in finite time intervals is developed in section 3. The different possible forms of the maps—particularly the so-called perturbed twist maps and symmetric maps—and their accuracy are discussed in section 4. In sections 5 and 6 the accuracy of the maps is studied for two examples of Hamiltonian systems: a simple fully integrable one and a non-integrable one, respectively. We also compared the mapping solutions with the exact solution and with the conventional symplectic integration method. A summary and conclusions are given in section 7. Calculations of the second-order generating function are presented in the appendix.

2. The Hamilton–Jacobi method for construction of maps

In this section we recall some basic principles of the Hamilton–Jacobi method for integrating Hamiltonian equations [1]—in particular, Jacobi's theorem—and derive a symplectic map describing the time evolution of the system. The idea of the Hamilton–Jacobi method is to find a canonical change of variables which reduces the Hamiltonian function to a form for which the Hamiltonian equations are integrable. The canonical transformation of variables is given by a generation function satisfying the Hamilton–Jacobi partial differential equation. If we succeed in finding a complete integral, i.e., the solution of this equation depending on n independent constants of motion ($2n$ is the number of variables), then the dynamics of the system will be determined by the generating function.

However, in many generic non-integrable Hamiltonian problems the system does not have n constants of motion, and the system may show chaotic behaviour. For these systems there is no complete integral of the Hamilton–Jacobi equation.

Nevertheless, Jacobi's theorem can be applied to these cases too, supposing that there exist approximately n integrals of motion in finite time intervals. Then the evolution of the system in each time interval is determined by Jacobi's theorem. By matching the orbits in the neighbouring time intervals, one can establish a long-term evolution of the system. Such a procedure replaces the canonical equations of motion by symplectic Hamiltonian maps.

2.1. The Hamilton–Jacobi equation and Jacobi's theorem

Let (q, p) $(q = (q_1, \ldots, q_n)$, $p = (p_1, \ldots, p_n))$ be canonical variables of the n-degree-of-freedom Hamiltonian system:

$$\frac{\mathrm{d}q}{\mathrm{d}t} = \frac{\partial H}{\partial p}, \qquad \frac{\mathrm{d}p}{\mathrm{d}t} = -\frac{\partial H}{\partial q}, \tag{1}$$

with $H = H(q, p, t)$ as the Hamiltonian function. Suppose that a change of variables $(q, p) \to (Q, P)$ given by the $2n$ functions $Q(q, p)$, $P(q, p)$ of the $2n$ variables q, p preserves certain invariants of the system and the form of the canonical equations (1) with a new Hamiltonian $\mathcal{H}$:

$$\frac{\mathrm{d}Q}{\mathrm{d}t} = \frac{\partial \mathcal{H}}{\partial P}, \qquad \frac{\mathrm{d}P}{\mathrm{d}t} = -\frac{\partial \mathcal{H}}{\partial Q}. \tag{2}$$

We consider that the change of variables is given by the generating function $S = S(q, P)$ for mixed variables, namely the old coordinates q and new momenta P:

$$p = \frac{\partial S(q, P, t)}{\partial q}, \qquad Q = \frac{\partial S(q, P, t)}{\partial P}, \qquad \mathcal{H} = H + \frac{\partial S(q, P, t)}{\partial t}, \tag{3}$$

and suppose that the new Hamiltonian $\mathcal{H}$ depends only on the canonical momenta P, i.e., $\mathcal{H} = \mathcal{H}(P)$. Then one can immediately integrate the Hamiltonian equations (2), which gives

$$Q = Q_0 + \Omega(P)(t - t_0), \qquad P = P_0 = \text{constant} \tag{4}$$

where $\Omega(P) = \partial \mathcal{H}(P)/\partial P$ is the oscillation frequency of the system in the new variables (Q, P). The generating function $S(q, P, t)$ satisfies the Hamilton–Jacobi equation

$$H\left(q, \frac{\partial S}{\partial q}, t\right) + \frac{\partial S}{\partial t} = \mathcal{H}(P). \tag{5}$$

As a partial differential equation, it may have a large number of solutions. The solution $S(q, P, t)$ of the Hamilton–Jacobi equation (5) which depends on the n independent constants $P_1, \ldots, P_n$ is called a complete integral of the equation if the following condition is satisfied: $\det(\partial^2 S/\partial q \partial P) \neq 0$.

Jacobi's theorem (see, e.g., [1]) states that *if a solution $S(q, P, t)$ is some complete integral of the Hamilton–Jacobi equation, then solutions of the canonical equations (1) may be represented by $p = \partial S/\partial q$, $Q = \partial S/\partial P$.*

This means that the time evolution of the system is completely determined by the generating function $S(q, P, t)$. For instance, suppose that (q_0, p_0) are the initial coordinates of the system at the time instant $t = t_0$. Then, by means of the canonical transformation $(q_0, p_0) \to (Q_0, P_0)$, equation (3), carried out by the generating function S at $t = t_0$, we can determine the corresponding new variables (Q_0, P_0). Since the time evolution of these variables is known (4), the original variables $(q(t), p(t))$ at any time moment $t > 0$ may be found by means of the backward canonical transformation $(Q(t), P(t)) \to (q(t), p(t))$, equation (3).

2.2. Canonical transformation and mapping

For non-integrable Hamiltonian systems, for which one cannot find a complete integral of the Hamilton–Jacobi equations, the evolution of the system does not obey Jacobi's theorem. Nevertheless, the idea of canonical transformations of variables may still be helpful for studying these non-integrable Hamiltonian systems. Below, we describe a procedure of canonical change of variables which reduces the canonical Hamiltonian equations to algebraic Hamiltonian maps.

We consider the generic Hamiltonian problem, namely the fully integrable system with Hamiltonian $H_0(q, p)$ subjected to the perturbation $\epsilon H_1(q, p, t)$ [1, 2]:

$$H = H(p, q, t) = H_0(q, p) + \epsilon H_1(q, p, t), \tag{6}$$

where ϵ is a perturbation amplitude. The unperturbed motion ($\epsilon = 0$) is integrable and therefore one can introduce the action $I = (I_1, \ldots, I_n)$ and angle variables $\theta = (\theta_1, \ldots, \theta_n) \pmod{2\pi}$ [1]. The unperturbed Hamiltonian is $H_0 = H_0(I)$ and the motion is conditionally periodic on the n-dimensional torus $I = (I_1, \ldots, I_n)$ with the frequencies $\omega(I) = \partial H_0(I)/\mathrm{d}\, I = (\omega_1, \ldots, \omega_n)$, i.e., $I =$ constant, $\theta = \theta_0 + \omega(I)(t - t_0)$.

The perturbed Hamiltonian $H_1(\theta, I, t)$ is a 2π-periodic function of the angular variables θ and it may be expanded in a Fourier series:

$$H_1(I, \theta, t) = \sum_{m,n} H_{mn}(I) \exp(\mathrm{i}m\theta - \mathrm{i}n\Omega t). \tag{7}$$

In the presence of a perturbation ($\epsilon \neq 0$), some (or all) of the integrals of motion $I = (I_1, \ldots, I_n)$ may be destroyed, and the system is non-integrable. In order to study the time evolution of the system in this case, we intend to construct a map

$$(\theta_{k+1}, I_{k+1}) = \hat{T}(\theta_k, I_k), \tag{8}$$

connecting the variables $\theta_k = \theta(t_k)$, $I_k = I(t_k)$ at the sequence of periodic time instants $t_k = 2\tau k$ ($k = 0, \pm 1, \pm 2, \ldots$) with a duration τ.

However, unlike in the canonical transformation over infinite time intervals (see section 2.1), we perform a change of variables $(\theta, I) \to (J, \Theta)$ only in the time interval $t_k < t < t_{k+1}$, i.e., the new Hamiltonian $\mathcal{H}$ is $\mathcal{H}(J)$ (and therefore $\Theta = \Theta_0 + \Omega(J, t')(t - t_0)$, $J =$ constant, $\Omega(J) = \mathrm{d}\mathcal{H}(J)/\mathrm{d}J$) in the interval $t_k < t < t_{k+1}$. The generating function $S(\theta, J, t)$ for such a transformation satisfies the Hamilton–Jacobi equation in this time interval:

$$H_0\left(\frac{\partial S}{\partial \theta}\right) + \epsilon H_1\left(\theta, \frac{\partial S}{\partial \theta}, t\right) + \frac{\partial S}{\partial t} = \mathcal{H}(J). \tag{9}$$

For the unperturbed system ($\epsilon = 0$), the generating function has the following expression:

$$S^{(0)}(\theta, J, t) = \theta J - H_0(J)t + \mathcal{H}(J, t)t, \tag{10}$$

and according to the Jacobi theorem the equations of motion are

$$I = \frac{\partial S^{(0)}(\theta, J, t)}{\partial \theta}, \qquad \Theta = \frac{\partial S^{(0)}(\theta, J, t)}{\partial J} = \theta - \omega t + \Omega(J)t, \tag{11}$$

where Θ and J are constants of motion. In the new variables (Θ, J), the equations of motion (2) are integrable and have the solutions (4). Then from (4) and (11) there follows the map

$$I_{k+1} = I_k, \qquad \theta_{k+1} = \theta_k + \omega(J)(t_{k+1} - t_k). \tag{12}$$

Consider the effect of perturbation supposing that the generating function in this case has an ansatz

$$S(\theta, J, t; \epsilon) = S^{(0)}(\theta, J, t) + \epsilon S^{(1)}(\theta, J, t; \epsilon), \tag{13}$$

where $\epsilon S^{(1)}(\theta, J, t; \epsilon)$ is the perturbation part of the generating function determined from the Hamilton–Jacobi equation (9). Then according to Jacobi's theorem the equations of motion are

$$\begin{aligned} I &= \frac{\partial S(\theta, J_k, t; \epsilon)}{\partial \theta} = J_k + \epsilon \frac{\partial S^{(1)}(\theta, J_k, t; \epsilon)}{\partial \theta}, \\ \Theta &= \frac{\partial S(\theta, J_k, t; \epsilon)}{\partial J_k} = \theta - \omega t + \Omega(J_k)t + \epsilon \frac{\partial S^{(1)}(\theta, J_k, t; \epsilon)}{\partial J_k}, \end{aligned} \tag{14}$$

where J_k is a constant of motion within the time interval $t_k \leqslant t \leqslant t_{k+1}$.

It follows from (14) that the coordinates $(\theta(t), I(t))$ of the trajectory at any moment of time t $(t_k \leqslant t \leqslant t_{k+1})$ with the initial coordinates (θ_k, I_k) at the time instant $t = t_k$ may be found by making successive canonical transformations: the first one transforms the original variables (θ_k, I_k) to the new ones (Θ_k, J_k), and the second one transforms (Θ_k, J_k) back to the old variables at the time instant t:

$$I_k = \frac{\partial S(\theta_k, J_k, t_k; \epsilon)}{\partial \theta_k}, \qquad \Theta_k = \frac{\partial S(\theta_k, J_k, t_k; \epsilon)}{\partial J_k}, \tag{15}$$

$$I(t) = \frac{\partial S(\theta(t), J_k, t; \epsilon)}{\partial \theta(t)}, \qquad \Theta(t) = \frac{\partial S(\theta(t), J_k, t; \epsilon)}{\partial J_k} = \Theta_k + \Omega(J_k)(t - t_k). \tag{16}$$

This allows us to construct the map (8) in the form

$$J_k = I_k - \epsilon \frac{\partial S_k^{(1)}}{\partial \theta_k}, \qquad \bar{\Theta}_k = \theta_k + \epsilon \frac{\partial S_k^{(1)}}{\partial J_k}, \tag{17}$$

$$\bar{\Theta}_{k+1} = \bar{\Theta}_k + \omega(t_{k+1} - t_k), \tag{18}$$

$$I_{k+1} = J_k + \epsilon \frac{\partial S_{k+1}^{(1)}}{\partial \theta_{k+1}}, \qquad \theta_{k+1} = \bar{\Theta}_{k+1} - \epsilon \frac{\partial S_{k+1}^{(1)}}{\partial J_k}, \tag{19}$$

where $\bar{\Theta}(t) = \Theta(t) + \omega(J)t$, and $S_k^{(1)} \equiv S^{(1)}(\theta_k, J_k, t_k; \epsilon)$, $S_{k+1}^{(1)} \equiv S^{(1)}(\theta_{k+1}, J_k, t_{k+1}; \epsilon)$.

One should note that the transformations in the forms (15), (16) are general and independent of the assumptions on the Hamiltonian function $H(\theta, I, t)$, like the ansatz (6). The forms (17), (19) of the map (8) are invariant with respect to a change of the time sequences $k \leftrightarrow k + 1$, i.e., the backward map $(\theta_{k+1}, I_{k+1}) \to (\theta_k, I_k)$ may be obtained from the forward map (8) by simply reversing the sequence of the canonical transformations. This also means that if $S^{(1)}(\theta_{k+1}, J_k, t_{k+1}) \neq 0$, then $S^{(1)}(\theta_k, J_k, t_k) \neq 0$.

3. The perturbation theory in finite time intervals

Determination of the generating function $S(\theta, J, t)$ by integrating the Hamilton–Jacobi equation (9) is a rather difficult task. The traditional methods used to study the Hamilton–Jacobi equation are based on perturbation theory [2,48]. The solutions are sought as a series in powers of the perturbation parameter ϵ for an unlimited time domain. However, these approaches encounter difficulties related to the divergence of the series due to the small denominators. Below, we present the version of the perturbation theory for the Hamilton–Jacobi equations in the finite time interval $t_k < t < t_{k+1}$ which does not encounter this problem.

Suppose for a moment that the perturbation parameter ϵ is small and we seek the generating function $S^{(1)}(\theta, J, t; \epsilon)$ as series in powers of ϵ:

$$S(\theta, J, t) = \theta J - H_0 t + \mathcal{H}(J; \epsilon)t + \epsilon S_1(\theta, J, t) + \epsilon^2 S_2(\theta, J, t) + \cdots. \tag{20}$$

Similarly, we expand the new Hamiltonian $\mathcal{H}(J; \epsilon)$ as well:

$$\mathcal{H}(J; \epsilon) = \mathcal{H}_0(J) + \epsilon \mathcal{H}_1(J) + \epsilon^2 \mathcal{H}_2(J) + \cdots. \tag{21}$$

Expanding the Hamilton–Jacobi equation (9) in a series in powers of ϵ and equating the terms of the same powers of ϵ, we obtain that $\mathcal{H}_0(J) = H_0(J)$ and the equations for the expansion coefficients $S_i \equiv S_i(\theta, J, t)$ of the generating function $S^{(1)}(\theta, J, t; \epsilon)$:

$$\frac{\partial S_1}{\partial t} + \frac{\partial H_0}{\partial J}\frac{\partial S_1}{\partial \theta} = \mathcal{H}_1(J) - H_1(\theta, J, t), \tag{22}$$

$$\frac{\partial S_i}{\partial t} + \frac{\partial H_0}{\partial J}\frac{\partial S_i}{\partial \theta} = \mathcal{H}_i(J) - F_i(\theta, J, t), \qquad i \geqslant 2, \tag{23}$$

where $F_i(\theta, J, t)$ are polynomial functions of derivatives $\partial S_1/\partial\theta, \ldots, \partial S_{i-1}/\partial\theta$. In particular, for $F_2(\theta, J, t)$ we have

$$F_2(\theta, J, t) = \frac{1}{2}\frac{\partial^2 H_0}{\partial J^2}\left(\frac{\partial S_1}{\partial \theta}\right)^2 + \frac{\partial H_1}{\partial J}\frac{\partial S_1}{\partial \theta}. \tag{24}$$

The equations (22), (23) should be complemented with the appropriate initial condition in the time interval $t_k < t < t_{k+1}$.

The equations (22), (23) for $S_i(\theta, J, t)$ are the first-order partial differential equations and may be solved by the method of characteristic equations. The right-hand sides of (22), (23) may be written as total time derivatives of $S_i \equiv S_i(\theta, J, t)$ taken along the trajectory $(\theta(t), J(t))$ determined by the unperturbed Hamiltonian $H_0(J)$, i.e., $\theta(t) = \theta_0 + \omega(J)(t - t_0)$, $J(t) =$ constant. Then the solutions of equations (22), (23) are

$$S_i(\theta, J, t) = S_{i0}(J) - \mathcal{H}_i(J)(t - t_0) - \int_{t_0}^{t} F_i(\theta(t'), J, t')\,\mathrm{d}t', \tag{25}$$

satisfying the initial condition $S_i(\theta, J, t) = 0$ at the time instant $t = t_0$. In (25), $\theta(t') = \theta + \omega(J)(t - t')$ is the unperturbed trajectory, and $S_{i0}(J)$ is an arbitrary function of J. One can take $S_{i0}(J) \equiv 0$. There are two parameters in (25): $\mathcal{H}_i(J)$ and a time parameter t_0 $(t_k \leqslant t_0 \leqslant t_{k+1})$ which should be appropriately chosen.

Suppose that the functions $F_i(\theta, J, t)$ have the following Fourier expansion:

$$F_i(\theta, J, t) = F_0^{(i)}(J) + \sum_{m\neq 0} F_{mn}^{(i)}(J)\exp(\mathrm{i}m\theta - \mathrm{i}n\Omega t). \tag{26}$$

Choosing $\mathcal{H}_i(J) = F_0^{(i)}(J)$, the solution (25) may be rewritten as

$$S_i(\theta, J, t) = -(t - t_0)\sum_{m,n} c(x_{mn})F_{mn}^{(i)}(J)\exp[\mathrm{i}(m\theta - n\Omega t)], \tag{27}$$

where $x_{mn} = [m\omega(J) - n\Omega](t - t_0)$ and $c(x) = a(x) + \mathrm{i}\,b(x)$, with

$$a(x) = \frac{1 - \cos x}{x}, \qquad b(x) = \frac{\sin x}{x}, \tag{28}$$

is a localized complex function near its origin $x = 0$. Its real $(a(x))$ and imaginary $(b(x))$ parts have finite values at $x = 0$ $(a(0) = 0, b(0) = 1)$ and decay for large values $|x| \gg 1$ as shown in figure 1.

For the perturbed part of the Hamiltonian $H_1(\theta, I, t)$, equation (7), the first-order generating function $S_1(\theta, J, t)$ takes the form

$$S_1(\theta, J, t) = -(t - t_0)\sum_{m,n} |H_{mn}(J)| \times [a(x_{mn})\sin(m\theta - n\Omega t + \chi_{mn}) + b(x_{mn})\cos(m\theta - n\Omega t + \chi_{mn})], \tag{29}$$

where $H_{mn}(J = |H_{mn}(J)|\exp(\mathrm{i}\chi_{mn})$. One should note that the determination of the higher-order generating functions $S_i(J, \theta, t)$ $(i \geqslant 2)$ requires rather complicated analytical calculations. We have calculated the second-order generating function $S_2(J, \theta, t)$ which is presented in the appendix.

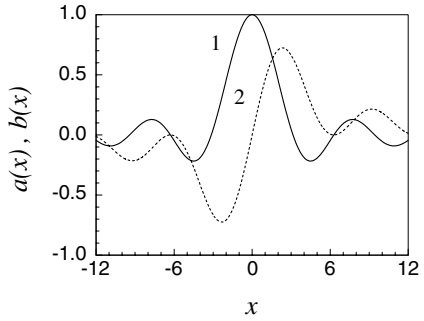

Figure 1. Oscillating functions $a(x)$ (curve 2) and $b(x)$ (curve 1).

Consider the expansion series near the resonant frequencies $(\omega(J), \Omega)$ $(m\omega(J) - n\Omega = 0)$ in more detail. From (27) and (29) it follows that the actual expansion parameter in the series (20) for the resonant values of J is not the perturbation parameter ϵ itself, but its combination with the time interval $(t - t_0)$, i.e., $\mu = \epsilon(t - t_0)^\nu$ with some exponent ν. The value of the exponent ν depends on the Hamiltonian perturbation $H_1(I, \theta, t)$ and usually $\nu \geqslant 1$. Indeed, the first term ϵS_1 in (20) is proportional to $\epsilon(t - t_0)$. The second-order generating function S_2 determined according to (25) and (24) gives $\epsilon^2 S_2 \sim \epsilon^2[c_1(t - t_0)^2 + c_2(t - t_0)^3]$, where c_1 and c_2 are coefficients $(c_1, c_2 \sim 1)$ (see the appendix). Similarly, for the higher-order terms in (20), one can at least have the estimates $\epsilon^n S_n \sim \epsilon^n(t - t_0)^n$, because the functions $F_i(\theta, J, t)$ $(i \geqslant 2)$ in (25) are polynomials in derivatives of lower-order generating functions $S_1, \ldots, S_{i-1}$ with respect to θ. As we will see in section 5, $\mu = \epsilon(t - t_0)^2$ for the simple Hamiltonian problem of particle motion in a perturbed field of a single wave. This nature of the expansion allows one to apply the perturbation theory to the generating function $S(\theta, J, t)$ not only for the small values of the perturbation parameter ϵ, but also for its large values, by taking a time interval $\tau = t_{k+1} - t_k$ which keeps the product $\mu = \epsilon(t - t_0)^\nu$ small.

It is interesting to compare the finite-time perturbation series with ones over infinite time intervals. The classical perturbation theory based on the Lindstedt's method gives the following solution of equations (22), (23) (see, e.g., [2]):

$$S_i(\theta, J, t) = -\sum_{m \neq 0} F_{mn}^{(i)}(J) \frac{\exp[\mathrm{i}(m\theta - n\Omega t)]}{\mathrm{i}(m\omega(J) - n\Omega)}, \tag{30}$$

containing the small denominators $(m\omega(J) - n\Omega)$ for numbers $(m, n) \neq 0$. The terms S_i are not defined for the values of J where the denominators $(m\omega(J) - n\Omega)$ are zero or too small. Small denominators may lead to the divergence of a series of the type of (20) and present fundamental difficulties in the perturbation theory.

Unlike (30), the finite-time perturbation series (20), (27), (29) do not contain divergent coefficients near the resonant frequencies $(\omega(J), \Omega)$ $(m\omega(J) - n\Omega = 0)$. The small denominators are replaced by the oscillating functions $a(x_{mn})$, $b(x_{mn})$, $x_{mn} = [m\omega(J) - n\Omega](t - t_0)$ which take finite values near the resonant frequencies $(\omega(J), \Omega)$. Due to the presence of the localized functions $a(x_{mn})$, $b(x_{mn})$, the main contribution to the perturbation series (20) at the given value of J comes just from the terms (m, n) for which $|(m\omega(J) - n\Omega)(t - t_0)| \leqslant \pi$. How can this property guarantee the convergence of the perturbation series and how does it depend on the time interval $t - t_0$? These problems are closely related to the KAM theory and it would require substantial efforts to resolve them.

4. The symmetric map and the perturbed twist maps

The generating functions determined in the previous section depend on the time parameter t_0. By appropriately choosing this parameter in the interval $[t_k, t_{k+1}]$, one can obtain different forms of the mapping. If $t_0 = t_{k+1}$, then the generating function $S^{(1)}(\theta, I, t)$ at the time instant $t = t_{k+1}$ is identically zero, i.e., $S^{(1)}(\theta_{k+1}, I_{k+1}, t_{k+1}) \equiv 0$. Then the map (17)–(19) takes the form

$$I_{k+1} = I_k - \epsilon \frac{\partial S^{(1)}}{\partial \theta_k}, \qquad \theta_{k+1} = \theta_k + \omega(I)\tau + \epsilon \frac{\partial S^{(1)}}{\partial I_{k+1}}, \tag{31}$$

($S^{(1)} \equiv S^{(1)}(\theta_k, I_{k+1}, t_k; \epsilon)$), known as *the perturbed twist map* [3,8]. Similarly, taking $t_0 = t_k$ one can obtain the alternative form the perturbed twist map:

$$I_{k+1} = I_k + \epsilon \frac{\partial S^{(1)}}{\partial \theta_{k+1}}, \qquad \theta_{k+1} = \theta_k + \omega(I)\tau - \epsilon \frac{\partial S^{(1)}}{\partial I_k}, \tag{32}$$

where $S^{(1)} \equiv S^{(1)}(\theta_{k+1}, I_k, t_{k+1}; \epsilon)$. These two forms of the perturbed twist map are not invariant with respect to the backward–forward transformations ($k \leftrightarrow k+1$).

Another important form of the map may be obtained by choosing the time parameter t_0 exactly at the middle of the time interval $[t_k, t_{k+1}]$, i.e. $t_0 = (t_k + t_{k+1})/2 = (k + 1/2)\tau$. Such a representation of the map (17)–(19) we call *the symmetric map*. The accuracy of the symmetric map is much higher than those of the perturbed twist maps. Indeed, the expansion parameter μ of the generating functions $S^{(1)}$ near the resonant frequencies for the symmetric map is $\mu = \epsilon(\tau/2)^\nu$, while for the perturbed twist maps (31), (32) it is equal to $\mu = \epsilon\tau^\nu$. Therefore, errors due to truncation of the power series of the generating function (20) in μ are smaller for the symmetric map than for the perturbed twist map. As we will see in the next section, the symmetric map gives excellent agreement with the exact behaviour of the Hamiltonian system.

The symmetric map is also invariant with respect to the change of time sequences $k \leftrightarrow k+1$, i.e., the backward map $(\theta_{k+1}, I_{k+1}) \to (\theta_k, I_k)$ may be obtained from the forward map (8) by simply reversing the sequence of the canonical transformations.

5. Example 1. Particle in a single-wave field

In order to study the accuracy of maps, we consider a simple, completely integrable Hamiltonian system, namely, a particle motion in a single-wave perturbation, i.e.,

$$H(\theta, I, t) = \frac{I^2}{2} - \epsilon \cos(\theta - \Omega t). \tag{33}$$

In a coordinate system running with the phase velocity of the wave, i.e., $q = \theta - \Omega t$, $p = I - \Omega$, it describes a pendulum with the frequency of the small-amplitude oscillations $\omega_0 = \sqrt{\epsilon}$. The corresponding Hamiltonian function $H_0(q, p) = H(q + \Omega t, I - \Omega, t)$ is a constant of the motion.

The system has the elliptic fixed points at $(y = 2\pi s, p = 0)$. The hyperbolic fixed points are at $(\theta = \pi(2s+1), p = 0)$ $(s = 0, \pm 1, \pm 2)$. For $-\omega^2 \leqslant H \leqslant \omega^2$ the motion is trapped and the trajectory is oscillating near the elliptic fixed points. The frequency of these non-linear oscillations is

$$\omega(H) = \frac{\pi\omega_0}{2K(k)}, \qquad k^2 = \frac{H + \omega_0^2}{2\omega_0^2}, \tag{34}$$

where $K(k)$ is the complete elliptic integral with a module k. For $H > \omega^2$ the motion is rotational.

We will consider the amplitude of the wave ϵ as a perturbation parameter. Then the unperturbed Hamiltonian $H_0(I) = I^2/2$ determines the unperturbed motion with the frequency $\omega(I) = \mathrm{d}H_0(I)/\mathrm{d}I = I$: $\theta = \theta_0 + \omega(I)(t - t_0)$, $I =$ constant.

5.1. The first- and second-order generating functions

According to (22), (26), and (29) the first-order generating function is

$$S_1(\theta, J, t) = -\frac{1}{\omega - \Omega}[\sin(\theta + \omega(t_0 - t) - \Omega t) - \sin(\theta - \Omega t)]$$
$$= (t - t_0)[a(x)\sin(\theta - \Omega t) + b(x)\cos(\theta - \Omega t)], \tag{35}$$

where $a(x)$ and $b(x)$ are oscillating functions (28), and $x = (J - \Omega)(t - t_0)$.

The second-order term $S_2(\theta, I, t)$ may be found according to (25) by integrating over the function $F_2(\theta, I, t)$, equation (24). Using the Hamiltonian $H_0(q, p)$ and the generating functions $S_1(\theta, J, t)$ (35), we obtain

$$F_2(\theta, J, t) = \frac{1}{2}\frac{\partial^2 H_0}{\partial J^2}\left(\frac{\partial S_1}{\partial \theta}\right)^2$$
$$= \frac{1}{4\omega^2}\frac{\partial^2 H_0}{\partial J^2}[2 - 2\cos[\omega(t - t_0)] + \cos[2\theta + 2\omega(t_0 - t) - 2\Omega t]$$
$$+ \cos(2\theta - 2\Omega t) - 2\cos[2\theta + \omega(t_0 - t) - 2\Omega t]]. \tag{36}$$

Integrating over the function (36) gives the second-order generating function $S_2(\theta, J, t)$ (see also the appendix):

$$S_2(J, \vartheta, t) = -\int_{t_0}^{t} F_2(J, \theta(t'), t')\,\mathrm{d}t'$$
$$= -\frac{(t - t_0)^3}{4}[A_0(x) + A_2(x)\sin(2\theta - 2\Omega t) + B_2(x)\cos(2\theta - 2\Omega t)], \tag{37}$$

where

$$A_0(x) = \frac{2}{x^2}\left[1 - \frac{\sin x}{x}\right], \tag{38}$$

$$A_2(x) = \frac{1}{x^2}\left[\sin 2x + \frac{1 - 4\cos x + 3\cos 2x}{2x}\right], \tag{39}$$

$$B_2(x) = \frac{1}{x^2}\left[\cos 2x + \frac{4\sin x - 3\sin 2x}{2x}\right] \tag{40}$$

are localized functions similar to the functions $a(x)$, $b(x)$, equation (28), in the Fourier expansion of the first-order generating function $S_1(J, \theta, t)$, equation (29). Note that the functions $A_0(x)$, $A_2(x)$, $B_2(x)$ are obtained from the localized functions $U(x, y)$, $V(x, y)$ of two variables (x, y) introduced in the appendix in the limits $x \to y$ and $x \to -y$, namely $A_0(x) = V(x, -x)$, $A_2(x) = U(x, x)$, $B_2(x) = V(x, x)$. Their plots are presented in figure 2. These functions have finite values at $x = 0$, i.e., at the resonant condition $\omega(J) - \Omega = 0$, and decay for large values of x.

The map (17)–(19) for the Hamiltonian system (33) may be rewritten in normalized variables (x, ϑ), $x = (J - \Omega)(t - t_0)$, $\vartheta = \theta - \Omega t$. Using (35), (37), the generating function $S^{(1)}$ for the corresponding map $(x_k, \vartheta_k) \to (x_{k+1}, \vartheta_{k+1})$ may be presented in the form

$$\epsilon S^{(1)}(\vartheta, x, t) = \mu S_1(\vartheta, x, t) + \mu^2 S_2(\vartheta, x, t) + \mathrm{O}(\mu^3), \tag{41}$$

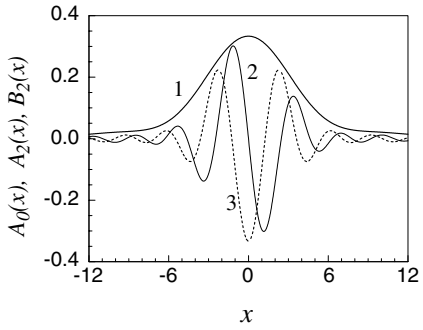

Figure 2. Oscillating functions $A_0(x)$ (curve 1), $A_2(x)$ (curve 2), and $B_2(x)$ (curve 3).

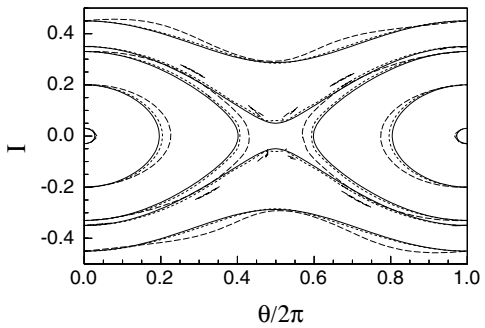

Figure 3. Several orbits of the Hamiltonian system (33) in the (θ, I) plane obtained from the symmetric map (dotted curves) and the perturbed twist map (dashed curves). Solid curves represent the exact orbits. The parameters are $\epsilon = 0.03$, $\Omega = 0$.

where

$$S_1(\vartheta, x, t) = a(x)\sin\vartheta + b(x)\cos\vartheta,$$
$$S_2(\vartheta, x, t) = -[A_0(x) + A_2(x)\sin 2\vartheta + B_2(x)\cos 2\vartheta].$$

Here $\mu = \epsilon(t - t_0)^2$ is an expansion parameter. As was mentioned in section 4, for the symmetric map the time instant $t_0 = (k + 1/2)\tau$ and therefore the expansion parameter $\mu = \epsilon\tau^2/4$. For the perturbed twist map the time $t_0 = t_{k+1}$ (or $t_0 = t_k$), and the corresponding expansion parameter is larger, i.e., $\mu = \epsilon\tau^2$.

5.2. Comparison of the symmetric map and the perturbed twist map

Before we made estimates of the accuracy of maps for the model (33), we compared the two forms of the map: the symmetric map (17)–(19) and the perturbed twist map (31). Several trajectories of the system in the phase plane (θ, I) obtained from the symmetric map and the perturbed twist map (31) are presented in figure 3 using the first-order generating function $S^{(1)} = S_1(I, \theta, t)$. The value of ϵ is taken equal to 0.03, and the map period τ is 2π. The initial conditions of trajectories were $(\theta_0, I_0) = (0, 0.03)$, $(0, 0.2)$, $(0, 0.33)$, $(0, \pm 0.35)$, $(0, \pm 0.45)$. Solid curves represent the exact trajectories of the pendulum; dotted curves and dashed curves correspond to the symmetric map and the perturbed twist map, respectively. As can be seen from figure 3, the symmetric map describes the trajectories much more closely than the perturbed twist map. The phase-space curves obtained from the symmetric map are

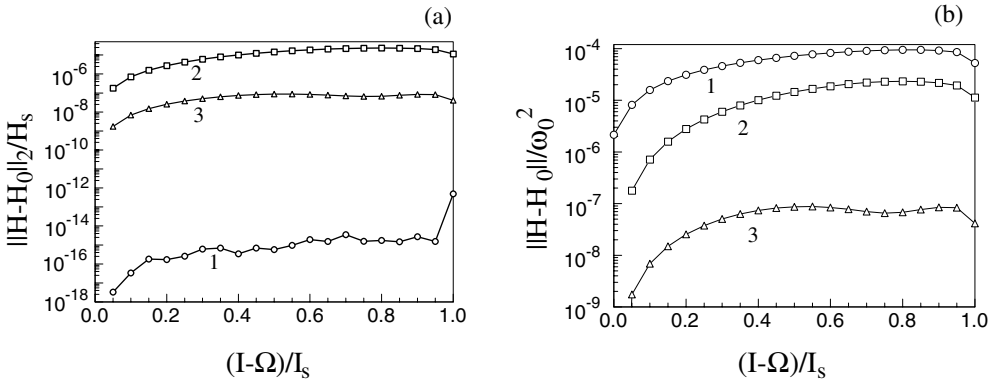

Figure 4. Relative root mean square energy errors $\|H - H_0\|_2/H_s$ ($H_s = \omega_0^2$) for the system (33) as a function of oscillation amplitude I. The parameter $\epsilon = \omega_0^2 = 0.01$. (*a*) Perturbation frequency $\Omega = 0$; (*b*) $\Omega = 1$. Curve 1 corresponds to the SI (see the text) with the integration step $\Delta t = \pi/100$. The time step of the map is $\tau = \pi$. Curve 2 corresponds to the map with the first-order generating function $S^{(1)} = S_1$, equation (35), and curve 3 to that with $S^{(1)} = S_1 + \epsilon S_2$, equation (37).

symmetric with respect to the axes $I = 0$ and $\theta = \pi$, similarly to the exact trajectories, while the trajectories of the perturbed twist map are asymmetric.

5.3. Accuracy of the symmetric map

The accuracy of the symmetric map is studied by integrating the Hamiltonian system (33) using the map and comparing the result with the exact solution. We also integrated the model (33) by standard symplectic integration methods. For this purpose, we have chosen one of the most accurate methods, namely the fifth-order explicit Runge–Kutta method that was developed by McLachlan and Atela [49]. The method was applied to the separable Hamiltonian of the form $H(p, q) = T(p) + V(q)$ with the quadratic kinetic part $T(p) = p^2/2$.

One should note that from the computational point view the symmetric mapping (17)–(19), as well as the perturbed twist mappings (31), are implicit methods. The variables J_k in the first set of equations (17) and θ_{k+1} in the second set of equations (19) are defined implicitly, and they should be found by solving corresponding algebraic equations. For this purpose we have used Newton's method (or the Newton–Raphson method) which has a high rate of convergence [50]. As an initial value in the iterative procedure, one can take I_k in the first equation of (17), and $\bar{\Theta}_{k+1}$ in the second equation of (19), because the differences $|J_k - I_k|$ and $|\bar{\Theta}_{k+1} - \theta_{k+1}|$ are of the order of the small expansion parameter μ, i.e., $\epsilon|\partial S^{(1)}/\partial\theta| \sim \mu \ll 1$.

We have considered two perturbations, a time-independent one ($\Omega = 0$) and a time-dependent one ($\Omega = 1$). The amplitude ϵ is taken equal to $\epsilon = \omega_0^2 = 0.01$. We have taken a set initial conditions ($\theta = 0$, $I = I_i$) ($\Omega \leqslant I_i \leqslant \Omega + I_s$) for the trapped orbits and integrated the system up to $t = 4\pi \times 10^4$ by means of the symmetric map and the symplectic integrator of McLachlan and Atela (abbreviated as SI). Here $I_s = 2\omega_0$ is the value of the amplitude I at the separatrix. The root mean square energy errors $\|H - H_0\|_2$ are calculated over all time instants $t_k = 2\pi k$ ($k = 1, \ldots, N = 2 \times 10^4$), i.e.,

$$\|H - H_0\|_2^2 = \frac{1}{N}\sum_{k=1}^{N}(H(\theta_k, I_k, t_k) - H_0)^2.$$

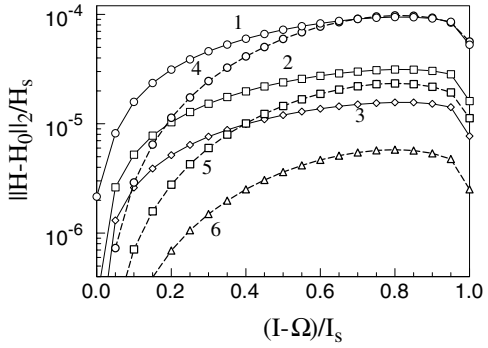

Figure 5. As figure 4, but for different integration steps of the SI and the symmetric map. Solid curves 1–3 correspond to the SI with the integration steps $\Delta t = \pi/100$, $\pi/300$, and $\pi/600$, respectively. Dashed curves 4–6 correspond to the map with the first-order generating function $S^{(1)} = S_1$ and the time steps $\tau = 2\pi$, π, and $\pi/2$, respectively. The other parameters are the same as in figure 4.

They are shown in figure 4 as a function of the oscillation amplitude I_i: (*a*) shows the time-independent case, $\Omega = 0$, and (*b*) the time-dependent case, $\Omega = 1$. The time step of the map is $\tau = \pi$, and the integration step of the SI is $\Delta t = \pi/100$. Curve 1 corresponds to the SI, and curves 2, 3 show the map results. Curve 2 corresponds to the map with the generating function $S^{(1)}$ at the first order of perturbation parameter ϵ, equation (35), i.e., $S^{(1)} = S_1$, and curve 3 corresponds the case where the second-order generating function S_2, equation (37), is included as well, i.e., $S^{(1)} = S_1 + \epsilon S_2$.

As one can see from figure 4, the energy errors of the SI in the time-independent case are several orders smaller than for the map. However, in the time-dependent case the accuracy of the SI is significantly reduced whereas the accuracy of the mapping has not been changed. Moreover, the energy errors of the SI become two orders higher than for the maps. Inclusion of the second order of the generating function S_2 improves the accuracy of the map by more than two or three orders. In particular, it reduces the energy error by a factor of 167 at the value of $(I - \Omega)/I_s = 0.5$. At this value of I the ratio of energy errors of the SI, the map with the first-order generating function, and that with the second-order generating function is 832:167:1 for the time-dependent case ($\Omega = 1$). Therefore, *the accuracy of the map at the fixed time step τ does not depend on the frequency* Ω, while the accuracy of the SI depends significantly on Ω and reduces with increasing Ω for a fixed integration step Δt.

One can reduce the energy errors by taking smaller integration steps Δt in the SI, as well as time steps τ in the map. This is shown in figure 5. Solid curves 1–3 correspond to the SI with the integration steps $\Delta t = 2\pi/200$, $2\pi/600$, and $2\pi/1200$, respectively. Dashed curves 4–6 correspond to the map with the first-order generating function $S^{(1)} = S_1$ and the time steps $\tau = 2\pi$, $2\pi/2$, and $2\pi/4$, respectively. The other parameters are the same as in figure 4(*b*). One should note that the energy errors of the SI, as well as those of the maps, are dependent on the amplitude of the oscillations $\delta I = I - \Omega$. The energy errors of the SI with the integration step $\Delta t = 2\pi/200$ are nearly the same as for the map with time step $\tau = 2\pi$. The computational time required for the map is almost one order shorter than that required for the SI.

The accuracy of the map and the SI are also studied by computing the non-linear oscillation frequency $\omega(I)$ of the trapped orbits and comparing it with the exact value $\omega_{\text{exact}}(I)$, equation (34). The relative difference of frequencies $\Delta\omega/\omega = [\omega(I) - \omega_{\text{exact}}(I)]/\omega$ is

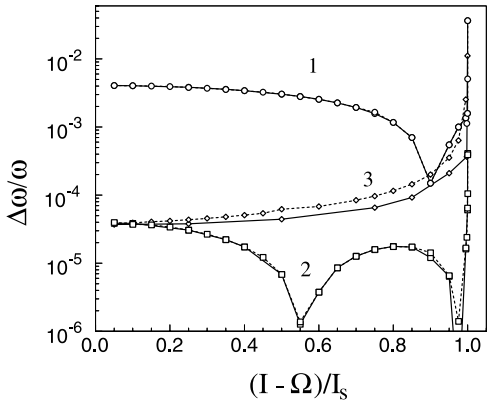

Figure 6. Relative differences $\Delta\omega(I)/\omega(I)$ between the non-linear oscillation frequency $\omega_m(I)$ calculated from the mapping and its exact value $\omega(I)$, equation (34), for different amplitudes of oscillations I. Solid curves: $\epsilon = 0.01$, $\tau = 2\pi/2$; dashed curves: $\epsilon = 1$, $\tau = 2\pi/10$. Curve 1 corresponds to the map with the generating function $S^{(1)} = S_1$, curve 2 to that with $S^{(1)} = S_1 + \epsilon S_2$. Curves 3 correspond to the SI with $\Delta t = \pi/100$. Frequency $\Omega = 1$.

plotted in figure 6 as a function of the relative oscillation amplitudes $(I - \Omega)/I_s$. The solid curves correspond to the perturbation $\epsilon = 0.01$, and the dashed curves to $\epsilon = 1$. The perturbation frequency is $\Omega = 1$ for both cases. The time step of the map is taken equal to $\tau = 2\pi/2$ for $\epsilon = 0.01$ and $\tau = 2\pi/20$ for $\epsilon = 1$. The solid and dashed curves 1 show results obtained from the mapping with the first-order generating function S_1, equation (35), and curves 2 correspond to the mapping with the first-order and second-order generating functions (37), i.e., $S^{(1)} = S_1 + \epsilon S_2$. Curve 3 shows the results for the SI with the integration step $\Delta t = 2\pi/200$.

First of all, we can see that the relative accuracy of the map for the large perturbation $\epsilon = 1$ and the short time step $\tau = 2\pi/20$ is the same as for the small perturbation $\epsilon = 0.01$ and the long time step $\tau = 2\pi/2$, because the expansion parameter $\mu = \epsilon\tau^2/4$ takes equal values for the two cases. Secondly, the difference $\Delta\omega/\omega$ obtained by the mapping decreases with increasing oscillation amplitude $\delta I = I - \Omega$, while it grows monotonically for the SI. Inclusion of the second-order generating function S_2 improves the accuracy of the map by more than two orders. For the small oscillation amplitude δI, the accuracy of the SI is two orders higher than for the map with $S^{(1)} = S_1$, and of the same order as for the map with $S^{(1)} = S_1 + \epsilon S_2$. However, in order to keep the same accuracy of the SI for the higher perturbation frequency $\Omega > 1$, one has to take even smaller integration steps Δt.

Therefore, for the exact integrable system we have shown that the symmetric map with large time steps τ of the order of the perturbation period $2\pi/\Omega$ ($\tau \sim 2\pi/\Omega$) can achieve the same higher-order accuracy of calculations as the powerful symplectic integration methods with integration steps Δt two orders smaller than τ.

6. Example 2. Standard Hamiltonian

The standard map is a basic model in Hamiltonian chaos theory and has important applications in the problems of plasma physics [9, 51]. However, in spite of its extensive applications and studies during the past two decades, no rigorous derivations of the standard map have been proposed so far. In this section we discuss this problem, considering an important model of the

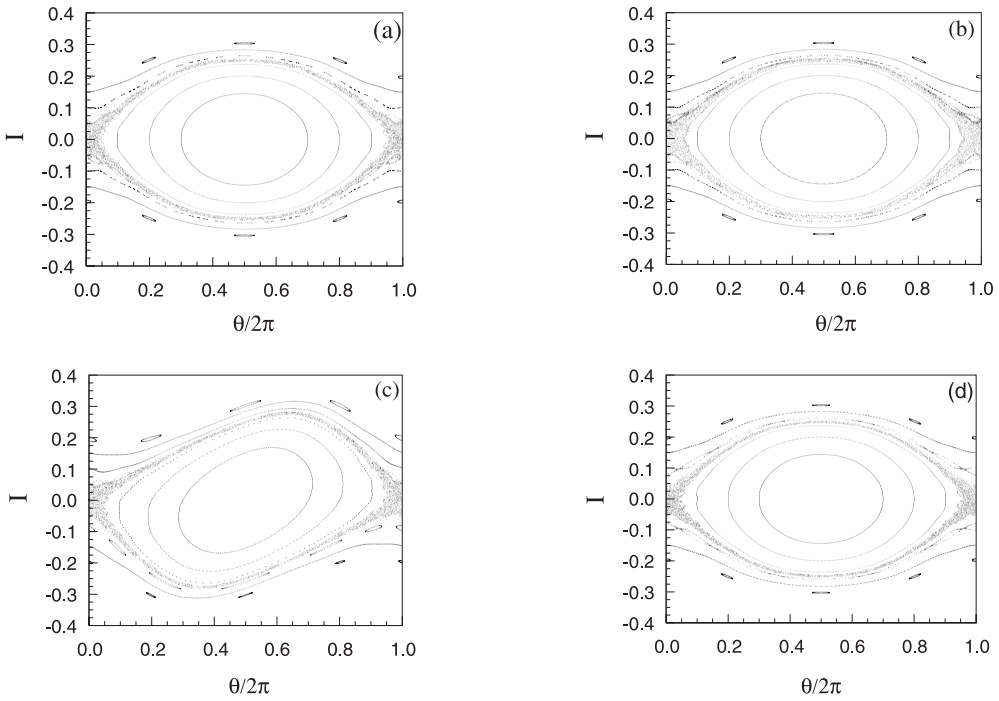

Figure 7. Poincaré sections for the standard Hamiltonian obtained by means of (*a*) the symplectic integrator with the time step $\Delta t = 2\pi/1100$; (*b*) the symplectic map with the period $\tau = 2\pi$; (*c*) the conventional standard map; (*d*) the symmetric standard map. The parameters are $K = 0.7$, $M = 10$.

non-integrable Hamiltonian system, namely the standard Hamiltonian (see, for example [51]):

$$H(I, \theta, t) = \frac{I^2}{2} + \frac{K}{4\pi^2} \sum_{n=-M}^{M} \cos(\theta - nt), \tag{42}$$

where K is the stochasticity (perturbation) parameter. The system (42), in particular, describes the motion of a particle in a wave field with a broad spectrum. It is widely assumed that in the limit of large number of modes $M \to \infty$, the system (42) is reduced to the celebrated Chirikov–Taylor map [3, 7]:

$$I_{s+1} = I_s + \frac{K}{2\pi} \sin\theta_s, \qquad \theta_{s+1} = \theta_s + 2\pi I_{s+1}, \tag{43}$$

where $(I_s, \theta_s) = (I(t = 2\pi s), \theta(t = 2\pi s))$ $(s = 0, \pm 1, \pm 2, \ldots)$. The derivation is based on the fact that in the limit $M \to \infty$ the sum of the right-hand side of (42) is reduced to the sum of an infinite number of the delta functions $\delta(t - t_s)$. However, the perturbation has singularities at the time instants $t = t_s$ and the variables I are not defined at these moments. By appropriately defining the integration along the delta function, one can obtain the standard map in the form (43) where $I_s = I(t = 2\pi s - 0)$, or in the form

$$\theta_{s+1} = \theta_s + 2\pi I_s, \qquad I_{s+1} = I_s + \frac{K}{2\pi} \sin\theta_{s+1}, \tag{44}$$

where $I_s = I(t = 2\pi s + 0)$. Both forms of the map (43), (44) may equivalently represent the standard Hamiltonian at the limit $M \to \infty$.

However, from the physical point of view one can expect these maps to closely describe the Hamiltonian system (42) for large but finite mode number M. As is shown in figure 7, the standard map (43) does not reproduce Poincaré sections of the system (42).

A mathematically correct and physically reasonable approach would consist of two steps: first, obtaining the map for the finite mode number M; and then, considering the limit $M \to \infty$. Such a method would avoid the uncertainty in the integration along the delta function. It has been shown quite recently in [45] that the usual procedure of canonical change of variables in the Hamiltonian (42) gives the symmetric standard map

$$J_s = I_s + \frac{K}{4\pi}\sin\theta_s, \qquad \theta_{s+1} = \theta_s + 2\pi J_s, \qquad I_{s+1} = J_s + \frac{K}{4\pi}\sin\theta_{s+1}, \tag{45}$$

for large $M \gg 1$. However, it was supposed that the perturbation parameter K was small, i.e., $\epsilon = K/2\pi \ll 1$. Below, using the method proposed in section 3, we will show that the symmetric standard map (45) is also valid for arbitrarily large values of K. The standard maps of the forms (43) and (44) may be obtained from the symmetric standard map (45) for the variables (J_s, θ_s).

We first study some properties of the generating function $S^{(1)}$, equation (29), of the system (42). It may be written in the form

$$S_1(J, \vartheta, t) = \sum_{n=-M}^{M} \frac{1}{J-n}\{\sin(\theta - (J-n)(t-t_0) - nt) - \sin(\theta - nt)\}. \tag{46}$$

Consider the asymptotic behaviour of $S_1(J, \vartheta, t)$ at the limit of large mode numbers $M \gg 1$. Using the formulae

$$\sum_{n=-\infty}^{\infty} \frac{\sin(nt+\alpha)}{J-n} = \frac{\pi}{\sin\pi J}\sin([t]J + \alpha), \qquad \sum_{n=-\infty}^{\infty} \frac{1}{J-n} = \frac{\pi}{\tan\pi J},$$

where $[t] = t - (2s+1)\pi$ and $2\pi s < t < 2\pi(s+1)$ $(s = 0, \pm1, \pm2, \ldots)$, one can show that for the arbitrary time instants t, t_0 in the interval $2\pi s < t, t_0 < 2\pi(s+1)$, the generating function $S_1(J, \vartheta, t)$ has the following asymptotics for large $M \gg 1$ (where $|J| \ll M$):

$$S_1(J, \vartheta, t) \sim \mathrm{O}(M^{-1}). \tag{47}$$

However, at the time instants $t = t_s = 2\pi s \pm 0$ and t_0 in the interval $2\pi s < t_0 < 2\pi(s+1)$, the generating function $S_1(J, \theta, t)$ has a finite asymptotic value for $M \gg 1$, i.e.,

$$S_1(\theta, J, t = 2\pi s \pm 0) = \pm\pi\cos\theta + \mathrm{O}(M^{-1}). \tag{48}$$

Then the second-order generating function $S_2(\theta, J, t)$ defined according to (24), (25), and (42) as

$$S_2(\theta, J, t) = -\int_{t_0}^{t} F_2(\theta(t'), J, t')\,\mathrm{d}t', \qquad F_2(\theta, J, t) = \left(\frac{\partial S_1}{\partial\theta}\right)^2, \tag{49}$$

goes to zero at all time instants t for $M \to \infty$. Similarly, the higher-order generating functions $S_i(\theta, J, t)$ $(i > 2)$ vanish as well, because the polynomial functions F_i of the derivatives $\partial S_1/\partial\theta, \ldots, \partial S_{i-1}/\partial\theta$ on the right-hand side of equations (23) tend to zero in the limit $M \to \infty$. Therefore, the generating function $S^{(1)}(\theta, J, t)$ of the symmetric map (17)–(19) is determined by the first-order generating function $S_1(\theta, J, t)$ for arbitrary perturbation parameter $\epsilon = K/4\pi^2$. The latter, determined by (48), gives the symmetric standard map (45).

Poincaré sections of the standard Hamiltonian (42), i.e., a sequence of phase-space coordinates (I_s, θ_s), are shown in figure 7 for the mode number $M = 10$ and the perturbation parameter $K = 0.7$: (a) obtained from the SI with the integration step $\Delta t = 2\pi/1100$; (b) corresponding to the symmetric map with the time step $\tau = 2\pi$; (c) corresponding to the

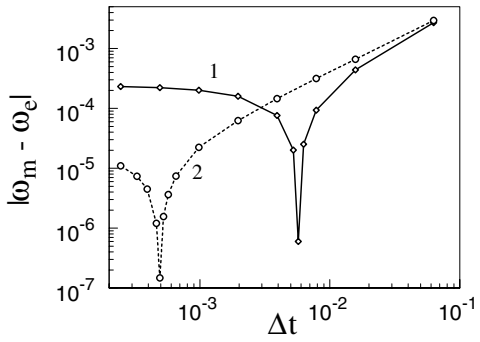

Figure 8. The difference $|\omega_m - \omega_e|$ between the oscillation frequencies of the regular trapped orbit of the standard Hamiltonian (42) calculated from the map (ω_m) and the SI (ω_e), as a function of the integration step of the SI Δt. Curve 1 corresponds to the map time step $\tau = 2\pi$, curve 2 to $\tau = 2\pi/64$. The initial coordinates of the orbit are $(I_0 = 2, \theta_0 = 0.6\pi)$. The parameters are $K = 1.5$, $M = 10$.

standard map (43), and (*d*) corresponding to the symmetric standard map (45). They are plotted with the same set of initial coordinates. One can see that the symmetric map reproduces well the Poincaré plot obtained from the SI. The symmetric standard map closely describes these plots, whereas the corresponding plot obtained by the standard mapping is asymmetrically deformed. The reason for this was explained in [45]; it is the case because the variables (I, θ) in the standard map (43) are not identical to the corresponding variables in the standard Hamiltonian (42).

For moderate values of the perturbation parameter $K \sim 1$, the motion of the standard Hamiltonian is partially chaotic, consisting of areas of chaotic as well as regular behaviour. First we study the accuracy of the symmetric map for regular orbits. For this we have computed the frequency of non-linear oscillation of the trapped regular orbit. We have chosen the perturbation parameter $K = 1.5$ and the mode number $M = 10$. At these parameter values the motion has both regular and chaotic components. We study the regular orbit with the initial coordinate at $(I_0 = 2, \theta_0 = 0.3)$. The difference between the frequencies $(|\omega_m - \omega_e|)$ calculated from the map (ω_m) and the SI (ω_e) is presented in figure 8 as a function of the integration step Δt of the SI. Curve 1 corresponds to the map time step $\tau = 2\pi$, and curve 2 to $\tau = 2\pi/64$. One can see that the accuracy of the map with the time step $\tau = 2\pi$ is the same as for the SI with the integration step $\Delta t = 2\pi/1200$, while the time step $\tau = 2\pi/64$ of the map corresponds to $\Delta t = 2\pi/12\,800$ for the SI. In the first case, the computational time required for the SI is 40 times longer than that required for the map, and in the second case it is five times longer.

The accuracy of the map was also tested by integrating the system forward in time up to a certain time instant t_{max}, then reversing it back in time to the initial time instant t_0. We checked how close the orbit comes to the initial point. The accuracy significantly depends on whether the orbit is regular or chaotic. For this test we have integrated the Hamiltonian system (42) with the initial coordinate (I_0, θ_0) from the time instant $t = 0$ up to $t = t_{max}$ and reversed it back in time. Let $I_f(t)$ and $I_b(t)$ be the components of the forward orbit and the backward orbit, respectively. The difference of these components $|I_f(t) - I_b(t)|$ is plotted in figure 9 as a function of $t_{max} - t$: (*a*) shows the case of the regular orbit with the initial coordinates $(I_0 = 2, \theta_0 = 0.6\pi)$; (*b*) corresponds to the chaotic orbit with coordinates $(I_0 = 2, \theta_0 = 0.02\pi)$.

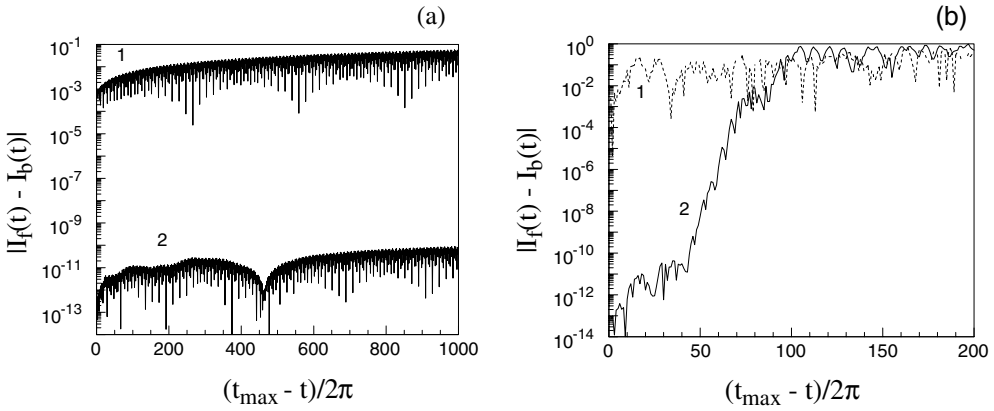

Figure 9. The accuracy of time reversal for the SI (curve 1) and the symmetric map (curve 2); (*a*) for the regular orbit; (*b*) for the chaotic orbit. The initial coordinates of the regular orbit are ($I_0 = 2, \theta_0 = 0.6\pi$), and those of the chaotic orbit are ($I_0 = 2, \theta_0 = 0.02\pi$). The integration step of the SI is $\Delta t = 2\pi/4000$; the map time step $\tau = 2\pi$, $t_{max} = 2\pi \times 10^3$. The other parameter are the same as for figure 8.

In both figures curve 1 describes the results for the SI with the integration step $\Delta t = 2\pi/4000$, and curve 2 is obtained for the map with the time step $\tau = 2\pi$. One can see from figure 9(*a*) that the accuracy of the map reversibility of the regular orbit is much higher than for the SI even with very small integration steps: for $t_{max} = 2\pi \times 10^3$ the regular orbit is reversed back to the initial point with accuracy less than 10^{-10}, while for the SI the accuracy is of the order of 10^{-2}.

From figure 9(*b*) it follows that the accuracy of the map is much higher too for the chaotic orbits than for the SI. However, due to an exponential growth of round-up operation errors, the time t_{max} for the reversal of the chaotic orbit to the initial point with the accuracy 10^{-10} is less than $t_{max} \approx 2\pi \times 50$. The reversibility of chaotic orbits for the SI is much poorer. The much better reversibility of the map is mainly due to its symmetric form, equations (17)–(19), which is invariant with respect to the map-reversing transformation $k \leftrightarrow k+1$, $H \to -H$. The latter property of the symmetric map expresses the invariance of the Hamiltonian equations (1) with respect to the formal time-reversing transformation $t \to -t$, $H \to -H$.

7. Conclusions

In summary, we have developed a general method for construction of maps for the Hamiltonian systems. It may be applied to the general class of Hamiltonian systems which may be composed as a sum of a fully integrable system and the Hamiltonian perturbation. The perturbation is not required to be small. The construction of the maps is based on the application of the Hamilton–Jacobi method—particularly the Hamilton–Jacobi equation and Jacobi's theorem—to the system in finite time intervals. The generating functions of the maps are solutions of the Hamilton–Jacobi equations in finite time intervals. They are found using the perturbation method by seeking the solutions as a series in powers of a small expansion parameter. It appears that the expansion parameter near the resonant frequencies is determined by the product of the perturbation parameter and the time step of the map. In particular, this allows one to apply the mapping method to a system with moderately large perturbation by taking the map time step sufficiently small.

We have studied the accuracy of the mapping method and compared it with those of the conventional symplectic integration methods, and in particular with the most accurate fifth-order Runge–Kutta symplectic integrator proposed by McLachlan and Atela [49]. It was found that the maps with large time steps comparable with the characteristic timescale of the system (e.g., a perturbation period) have the same accuracy as the symplectic integrator with integration steps two or three orders smaller. It is even more important that the accuracy of the map is not dependent on the perturbation frequency, and thus one can integrate highly oscillatory Hamiltonian systems—which is a challenging problem in numerical analysis [52].

We have left open some problems concerning the convergence of the finite-time perturbation series and the transition from finite times to infinite ones. The study of these problems is closely related to the perturbation theory for conditionally periodic motion of a system over infinite time intervals—the KAM theory—and requires special investigation.

Acknowledgments

The author gratefully acknowledges valuables discussions with Professor Gert Eilenberger. He also greatly appreciates the long-term support of this activity by him and by Professor Ulrich Samm. He also thanks Dr G Fuchs for reading the manuscript and useful suggestions.

Appendix. The second-order generating function

Here we calculate the second-order generating function $S_2(J, \theta, t)$ for the Hamiltonian function:

$$\begin{aligned} H(I, \vartheta, t) &= H_0(I) + \epsilon H_1(I, \vartheta, t), \\ H_1(I, \vartheta, t) &= \epsilon \sum_m H_m(I) \cos(m \cdot \vartheta + \chi_m), \end{aligned} \tag{A.1}$$

where $\vartheta = (\theta_1, \ldots, \theta_n, \Omega t)$, $m = (m_1, \ldots, m_n, n)$, $m \cdot \vartheta = m \cdot \theta + n\Omega t$. We write the first-order generating function $S_1(J, \vartheta, t)$ in the form

$$\begin{aligned} S_1(J, \vartheta, t) &= -\int_{t_0}^{t} H_1(J, \vartheta(t'), t')\, \mathrm{d}t' \\ &= \sum_m \frac{H_m(J)}{m \cdot \omega} [\sin(m \cdot \vartheta + m \cdot \omega(t_0 - t) + \chi_m) - \sin(m \cdot \vartheta + \chi_m)]. \end{aligned} \tag{A.2}$$

According to (23) and (24), the second-order generating function $S_2(J, \theta, t)$ is

$$S_2(J, \vartheta, t) = -\int_{t_0}^{t} F_2(J, \vartheta(t'), t')\, \mathrm{d}t', \tag{A.3}$$

where

$$F_2(I, \vartheta, t) = \frac{1}{2} \frac{\partial^2 H_0}{\partial J_i \, \partial J_j} \frac{\partial S_1}{\partial \vartheta_i} \frac{\partial S_1}{\partial \vartheta_j} + \frac{\partial H_1}{\partial J_i} \frac{\partial S_1}{\partial \vartheta_i}. \tag{A.4}$$

In (A.4), summation over repeated indices i, j ($i, j = 1, \ldots, n$) is assumed. Putting (A.1) and (A.2) into (A.4), we obtain

$$\begin{aligned} F_2(J, \vartheta, t) = \frac{1}{2} \sum_{m,m'} m_i \frac{\partial^2 H_0^{(1)}}{\partial J_i J_j} m'_j \frac{H_m(J) H_{m'}(J)}{m \cdot \omega \, m' \cdot \omega} \\ \times [\cos(m \cdot \vartheta + m \cdot \omega\,(t_0 - t) + \chi_m) - \cos(m \cdot \vartheta + \chi_m)] \\ \times [\cos(m' \cdot \vartheta + m' \cdot \omega\,(t_0 - t) + \chi_{m'}) - \cos(m' \cdot \vartheta + \chi_{m'})] \end{aligned}$$

$$+\sum_{m,m'} m'_j \frac{\partial H_m}{\partial J_j}\frac{H_{m'}(J)}{m'\cdot\omega}\cos(m\vartheta+\chi_m)$$
$$\times[\cos(m'\cdot\vartheta+m'\cdot\omega\,(t_0-t)+\chi_{m'})-\cos(m'\cdot\vartheta+\chi_{m'})]. \tag{A.5}$$

We replace the products of the trigonometric functions in (A.5) by their sum and integrate each of them using the integral

$$F_{ms}=\int_{t_0}^{t} \mathrm{d}t'\cos(m\cdot\vartheta(t')+s\cdot\omega(t_0-t')+\chi)$$
$$=a(x_m,x_s)\sin(m\cdot\vartheta+\chi)+b(x_m,x_s)\cos(m\cdot\vartheta+\chi), \tag{A.6}$$

where $x_m=m\cdot\omega(t-t_0)$ and

$$a(x,y)=-(t-t_0)\frac{\cos x-\cos y}{x-y},\qquad b(x,y)=(t-t_0)\frac{\sin x-\sin y}{x-y}.$$

Then, combining the trigonometric functions, we obtain the following expression for the generating function (A.3):

$$S_2(I,\vartheta,t)=-\frac{(t-t_0)^3}{4}\sum_{m,m'} m_i\frac{\partial^2 H_0}{\partial J_i\,\partial J_j}m'_j H_m(J)H_{m'}(J)$$
$$\times\{A^{(+)}_{m,m'}\sin(m+m')\cdot\vartheta+B^{(+)}_{m,m'}\cos(m+m')\cdot\vartheta$$
$$+A^{(-)}_{m,m'}\sin(m-m')\cdot\vartheta+B^{(-)}_{m,m'}\cos(m-m')\cdot\vartheta\}$$
$$-\frac{(t-t_0)^2}{2}\sum_{m,m'} m'_j\frac{\partial H_m(J)}{\partial J_j}H_{m'}(J)$$
$$\times\{C^{(+)}_{m,m'}\sin(m+m')\cdot\vartheta+D^{(+)}_{m,m'}\cos(m+m')\cdot\vartheta$$
$$+C^{(-)}_{m,m'}\sin(m-m')\cdot\vartheta+D^{(-)}_{m,m'}\cos(m-m')\cdot\vartheta\}, \tag{A.7}$$

where the coefficients $A^{(\pm)}_{m,m'}$, $B^{(\pm)}_{m,m'}$, $C^{(\pm)}_{m,m'}$, and $D^{(\pm)}_{m,m'}$:

$$A^{(+)}_{m,m'}=U(x_m,x_{m'}),\qquad A^{(-)}_{m,m'}=-U(x_m,-x_{m'}),$$
$$B^{(+)}_{m,m'}=V(x_m,x_{m'}),\qquad B^{(-)}_{m,m'}=-V(x_m,-x_{m'}), \tag{A.8}$$

$$C^{(+)}_{m,m'}=W(x_m,x_{m'}),\qquad D^{(+)}_{m,m'}=Y(x_m,x_{m'}),$$
$$C^{(-)}_{m,m'}=-W(x_m,-x_{m'}),\qquad D^{(-)}_{m,m'}=-Y(x_m,-x_{m'}), \tag{A.9}$$

are expressed in terms of four functions $U(x,y)$, $V(x,y)$, $W(x,y)$, and $Y(x,y)$ of two variables x, y:

$$U(x,y)=\frac{1}{xy}\left[\sin(x+y)+\frac{\cos(x+y)-\cos y}{x}+\frac{\cos(x+y)-\cos x}{y}+\frac{1-\cos(x+y)}{x+y}\right] \tag{A.10}$$

$$V(x,y)=\frac{1}{xy}\left[\cos(x+y)-\frac{\sin(x+y)-\sin y}{x}-\frac{\sin(x+y)-\sin x}{y}+\frac{\sin(x+y)}{x+y}\right] \tag{A.11}$$

$$W(x,y)=-\frac{1}{y}\left[\frac{\cos(x+y)-\cos y}{x}+\frac{1-\cos(x+y)}{x+y}\right] \tag{A.12}$$

$$Y(x,y)=\frac{1}{y}\left[\frac{\sin(x+y)-\sin y}{x}-\frac{\sin(x+y)}{x+y}\right]. \tag{A.13}$$

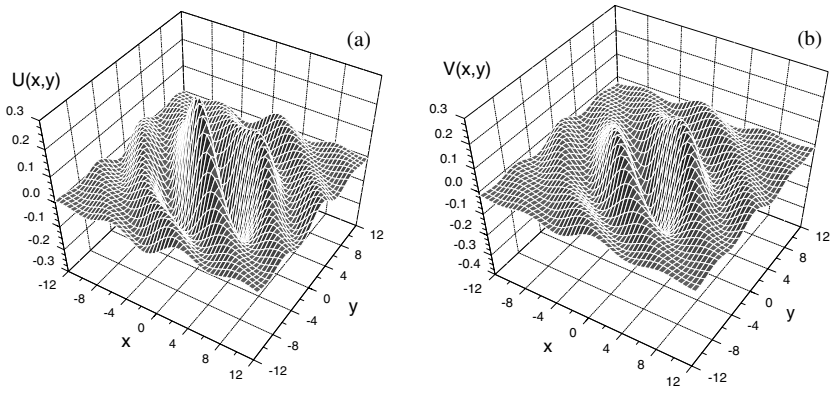

Figure A.1. Functions (*a*) $U(x, y)$ and (*b*) $V(x, y)$.

These functions have the following asymptotics at $y \to x$:

$$U(x, x) = \frac{1}{x^2}\left[\sin 2x + \frac{1 - 4\cos x + 3\cos 2x}{2x}\right] \tag{A.14}$$

$$V(x, x) = \frac{1}{x^2}\left[\cos 2x + \frac{4\sin x - 3\sin 2x}{2x}\right], \tag{A.15}$$

$$U(x, -x) = 0, \qquad V(x, -x) = \frac{2}{x^2}\left[1 - \frac{\sin x}{x}\right]. \tag{A.16}$$

The functions $U(x, y)$, $V(x, y)$, $W(x, y)$, and $Y(x, y)$ of the two variables x, y are localized in the finite region $|x| \leqslant \pi$, $|y| \leqslant \pi$. They decay at large values of x, y. The functions $U(x, y)$, $V(x, y)$ are shown in figure A.1.

References

[1] Arnold V I 1989 *Mathematical Methods of Classical Mechanics* (Berlin: Springer) ch 9
[2] Arnold V I, Kozlov V V and Neishtadt A I 1988 Mathematical aspects of classical and celestial mechanics *Dynamical Systems (Encyclopaedia of Mathematical Sciences vol 3)* (Berlin: Springer) ch 5
[3] Lichtenberg A J and Lieberman M A 1983 *Regular and Stochastic Motion* (New York: Springer) ch 3
[4] Sanz-Serna J M 1992 Symplectic integrators for Hamiltonian problems: an overview *Acta Numerica* (Cambridge: Cambridge University Press) pp 243–86
[5] Cartwright J H E and Piro O 1992 *Int. J. Bifurcation Chaos* **2** 427–49
[6] Feng K and Wang D-L 1994 *Contemporary Mathematics* vol 163, ed Z-C Shi and C-C Yang (Providence, RI: American Mathematical Society)
[7] Chirikov B V 1979 *Phys. Rep.* **52** 265
[8] Meiss J D 1992 *Rev. Mod. Phys.* **64** 795–848
[9] MacKay R S and Meiss J D (ed) 1987 *Hamiltonian Dynamical Systems—A Reprint Selection* (Bristol: Hilger)
[10] Rechester A B and White R B 1980 *Phys. Rev. Lett.* **44** 1586–9
[11] Rechester A B, Rosenbluth M N and White R B 1981 *Phys. Rev.* A **23** 2664–72
[12] Escande D F 1988 Plasma theory and nonlinear and turbulent processes in physics *Proc. Int. Workshop (Kiev, 1987)* ed V G Bar'yakhtar *et al* (Singapore: World Scientific) pp 398–430
[13] Cary R and Littlejohn R G 1983 *Ann. Phys., NY* **151** 576
[14] Boozer A H 1983 *Phys. Fluids* **26** 1288
[15] Martin T J and Taylor J B 1984 *Plasma Phys. Control. Fusion* **26** 321–40
[16] Wobig H 1987 *Z. Naturf.* a **42** 1054–66
[17] Wobig H and Fowler R H 1988 *Plasma Phys. Control. Fusion* **30** 721–41
[18] Bazzani A *et al* 1989 *Nuovo Cimento* **103** 659–68
[19] Viana R L and Caldas I L 1992 *Z. Naturf.* a **47** 941–4

[20] Punjabi A, Verma A and Boozer A 1992 *Phys. Rev. Lett.* **69** 3322–5
[21] Punjabi A, Ali H and Boozer A 1997 *Phys. Plasmas* **4** 337–46
[22] Abdullaev S S and Zaslavsky G M 1995 *Phys. Plasmas* **2** 4532–44
[23] Abdullaev S S and Zaslavsky G M 1996 *Phys. Plasmas* **3** 516–28
[24] Abdullaev S S, Finken K H, Kaleck A and Spatschek K H 1998 *Phys. Plasmas* **5** 196–210
[25] Balescu R, Vlad M and Spineanu F 1998 *Phys. Rev.* E **58** 951–64
[26] Balescu R 1998 *Phys. Rev.* E **58** 3781–92
[27] Fischer O and Cooper W A 1998 *Plasma Phys. Rep.* **24** 727–31
[28] Wobig H and Pfirsch D 2001 *Plasma Phys. Control. Fusion* **43** 695–716
[29] da Silva E S, Viana R L and Caldas I L 2001 *IEEE Trans. Plasma Sci.* **29** 617–631
[30] Horton W *et al* 1998 *Phys. Plasmas* **5** 3910–17
[31] Kwon J M *et al* 2000 *Phys. Plasmas* **7** 1169–80
[32] Weiss J B and Knobloch E 1989 *Phys. Rev.* A **40** 2579–89
[33] Weiss J B 1991 *Phys. Fluids* A **3** 1379–84
[34] del-Castillo-Negrete D and Morrison P J 1993 *Phys. Fluids* A **5** 948–65
[35] Weiss J B 1994 *Physica* D **76** 230–8
[36] Ahn T and Kim S 1994 *Phys. Rev.* E **51** 2900–11
[37] del-Castillo-Negrete D 1998 *Phys. Fluids* A **10** 576–94
[38] Berg J S, Warnock R L, Ruth R D and Forest É 1994 *Phys. Rev.* E **49** 722–39
[39] Dragt A J 1996 *Part. Accel.* **55** 253–84
[40] Wisdom J 1982 *Astron. J.* **87** 577–93
[41] Wisdom J and Holman M 1991 *Astron. J.* **102** 1528–38
[42] Wisdom J, Holman M and Touma J 1996 *Integration Algorithms for Classical Mechanics (Fields Institute Communications vol 10)* ed J E Marsden, G W Patrick and W F Shadwick (Providence, RI: American Mathematical Society) pp 217–44
[43] Zaslavsky G M, Sagdeev R Z, Usikov D A and Chernikov A A 1991 *Weak Chaos and Quasiregular Patterns* (Cambridge: Cambridge University Press)
[44] Eberhard M 1999 *Europhys. Conf. Abstracts J.* **23** 781–4
[45] Abdullaev S S 1999 *J. Phys. A: Math. Gen.* **32** 2745–66
[46] Abdullaev S S, Finken K H and Spatschek K H 1999 *Phys. Plasmas* **6** 153–74
[47] Bogolyubov N N and Mitropol'skij Yu A 1958 *Asymptotic Methods in the Theory of Nonlinear Oscillations* 2nd edn (Moscow: Nauka) (Engl. transl. 1961 (New York: Gordon and Breach))
[48] Ali N 1973 *Perturbation Methods* (New York: Wiley)
[49] McLachlan R I and Atela P 1992 *Nonlinearity* **5** 541–62
[50] Press W H, Teukolsky S A, Vetterling W T and Flannery B P 1992 *Numerical Recipes in C. The Art of Scientific Computing* 2nd edn (Cambridge: Cambridge University Press)
[51] Benisti D and Escande D F 1998 *Phys. Rev. Lett.* **80** 4871–4
[52] Petzold L R, Jay L O and Yen J 1997 Numerical solutions of highly oscillatory ordinary differential equations *Acta Numerica* (Cambridge: Cambridge University Press) pp 437–83